Tracing water masses with [129]I and [236]U in the subpolar North Atlantic along the GEOTRACES GA01 section

Maxi Castrillejo[1,2], Núria Casacuberta[1,3], Marcus Christl[1], Christof Vockenhuber[1], Hans-Arno Synal[1],
Maribel I. García-Ibáñez[4,5], Pascale Lherminier[6], Géraldine Sarthou[7], Jordi Garcia-Orellana[2] and Pere
Masqué[2,8]

[1]Laboratory of Ion Beam Physics, ETH-Zurich, Otto Stern Weg 5, Zurich, 8093, Switzerland

[2]Institut de Ciència i Tecnologia Ambientals & Departament de Física, Universitat Autònoma de Barcelona, Bellaterra, 08193,
Spain

[3]Institute of Biogeochemistry and Pollutant Dynamics, Environmental Physics, ETH-Zurich, Universitätstrasse 16, Zurich,
8092, Switzerland

[4]Uni Research Climate, Bjerknes Centre for Climate Research, Bergen 5008, Norway

[5]Instituto de Investigaciones Marinas (IIM-CSIC), Eduardo Cabello 6, 36208 Vigo, Spain

[6]Ifremer, Univ. Brest, CNRS, IRD, Laboratoire d' Océanographie Physique et Spatiale, IUEM, Plouzané, France

[7]Laboratoire des Sciences de l'Environnement Marin (LEMAR), UMR 6539, IUEM, Technopôle Brest Iroise, 29280 Plouzané,
France

[8]School of Science, Centre for Marine Ecosystems Research, Edith Cowan University, Joondalup, WA 6027, Australia

Correspondence to: Maxi Castrillejo (maxic@phys.ethz.ch)

Abstract.

The distribution of ^{129}I and ^{236}U in 14 depth profiles and the sea surface along the GEOVIDE section (transect GEOTRACES

5 GA01) the subpolar North Atlantic (SPNA) is presented for spring 2014. This work investigates the use of ^{129}I and ^{236}U as circulation tracers of water masses involved in the North Atlantic Meridional Overturning Circulation. The results show that ^{129}I and ^{236}U were distributed by water masses spanning ^{129}I concentrations, ^{236}U/^{238}U atom ratios and ^{129}I/^{238}U atom ratios of $(0.2 - 256) \times 10^7$ at/kg, $(40 - 2350) \times 10^{-12}$ and $0.5 - 200$, respectively. The highest tracer levels were associated with shallow waters carried by the East Greenland Current (EGC) and the Labrador Current (LC), as well as with the overflow waters

10 ventilating the deep SPNA. The presence of these radionuclides in the SPNA is mainly due to global fallout and varying contributions from nuclear reprocessing plants located near Sellafield, United Kingdom, and La Hague, France (0.1 % to > 5 %). Results show that part of the effluents discharged from Sellafield and La Hague apparently enter the eastern SPNA directly through the Iceland-Scotland passage or the English Channel/Irish Sea, as it is shown by elevated ^{129}I concentrations and ^{129}I/^{238}U ratios in shallow central waters flowing in the West European Basin (WEB). The ^{236}U/^{238}U and ^{129}I/^{238}U ratios help

15 identifying Arctic waters of Atlantic origin (PIW-Atlantic) in the EGC and of Pacific origin (PIW-Pacific) in the LC. PIW-Atlantic (PIW-Pacific) enriched in ^{129}I (in ^{236}U) appear to cascade along the slopes of Greenland and Newfoundland contributing to the overflows in the Irminger and Labrador Seas, respectively. The Iceland-Scotland Overflow Water spreading pathways into the eastern SPNA have been confirmed by the unequivocal transport of reprocessing ^{129}I into the deep WEB. Data of ^{129}I and ^{236}U from 2014 and the ^{129}I time series in the Labrador Sea agrees with the hypothesis that Atlantic Waters

20 (tagged with nuclear reprocessing plant effluents) follow at least two circulation loops from their source region: one short loop through the Nordic Seas into the SPNA of about 8 - 10 years, and a second, long loop, which adds about 8 years more of recirculation in the Arctic Eurasian Basin.

30

1 Introduction

The subpolar North Atlantic (SPNA) is a key region for the global oceanic circulation (all acronyms are described in Table 1). The North Atlantic Current (NAC) carries warm subtropical waters northwards to the SPNA, where they are transformed into cold Subpolar Mode Water (SPMW) and ultimately into Labrador Sea Water (LSW), which circulates southwards along with

5 the overflow waters from the Nordic Seas (Figure 1). These water mass formation processes constitute the starting point of the Atlantic Meridional Overturning Circulation (AMOC). Among other studies, the repeated hydrographic cruises along the Greenland-Portugal OVIDE line shed light on the decadal variability of the AMOC (Daniault et al., 2016; Lherminier et al., 2010; Mercier et al., 2013) and its relevance for climate by, for example, controlling the oceanic uptake of CO_2 (Pérez et al., 2013). The GEOVIDE cruise carried out in spring 2014 covered the OVIDE line and the Labrador Sea revealing an intense

10 AMOC over a cold and fresh SPNA (Zunino et al., 2017). The observed strong AMOC was linked to an intensified poleward transport of subtropical waters, as well as, to the increased equatorward transport of Iceland-Scotland Overflow Water (ISOW), Irminger-SPMW (IrSPMW) and Polar Intermediate Water (PIW) in 2014 relative to mean 2002 - 2010 (García-Ibáñez et al., 2018).

15 Anthropogenic tracers can provide complementary information about water mass circulation changes in the SPNA. For example, chlorofluorocarbons and sulphur hexafluoride from industrial activities, or tritium from atmospheric nuclear weapon tests (global fallout, GF) carried out in the 1950s and 1960s, allow understanding ventilation of the interior Atlantic Ocean (Doney and Jenkins, 1994; Sy et al., 1997; Tanhua et al., 2005). Contrary to chlorofluorocarbons or tritium, which were introduced into the surface ocean from rather well mixed atmosphere, nuclear reprocessing plants (NRPs) represent point-like

20 sources of artificial radionuclides. The RPs located near La Hague and Sellafield discharge(d) liquid effluents to the English Channel and the Irish Sea, respectively, over the past 50 - 60 years, thereby tagging Atlantic Waters (AWs) passing by these locations from the 1960s on (Kershaw and Baxter, 1995). Artificial radionuclides from NRPs (e.g., ^{137}Cs, ^{99}Tc, ^{129}I, ^3H etc.) have been used to investigate the spreading of AW through the Nordic Seas into the Arctic Ocean, and ultimately to the western North Atlantic Ocean (e.g. Aarkrog et al., 1983, 1987, Alfimov et al., 2004, 2013; Beasley et al., 1998; Casacuberta et al.,

25 2016; Christl et al., 2015b; Dahlgaard, 1995; Edmonds et al., 2001; Holm et al., 1983; Smith et al., 1998, 2005, 2011, 2016).

Iodine-129 ($T_{1/2}$ = 15.7 Ma) is regarded as a tracer particularly well suited for studying the water mass circulation in the SPNA because its input is dominated by releases from the European NRPs and they are well documented (He et al., 2013; Raisbeck et al., 1995). This isotope can be detected far away from the source region due to its conservative behaviour in seawater, the

30 long half-life and the low detection limits obtained with accelerator mass spectrometry (AMS) (e.g. Vockenhuber et al., 2015), providing information of upstream changes in ocean circulation. Overall, the magnitude and timing of ^{129}I discharges made this tracer valuable for investigating water mass transport pathways, advection and mixing, and for testing the performance of ocean circulation models in the Arctic and Atlantic Oceans (Karcher et al., 2012; Orre et al., 2010; Smith et al., 2016). In the

SPNA (Figure 1), most of the ^{129}I is nowadays present in Denmark Strait Overflow Water (DSOW) that overflows the sill between Greenland and Iceland, flowing southwards within the Deep Western Boundary Current (DWBC) (Smith et al., 2005, 2016) or following other interior pathways along the western equatorial Atlantic Ocean (Smith et al., 2016). The other overflow water, ISOW, enters the North Atlantic through the Iceland-Scotland Sill (Hansen and Osterhus, 2000) carrying comparably

5   less ^{129}I (Edmonds et al., 2001), yet its ^{129}I concentrations at the sill have increased 400 % over the last 20 years (Alfimov et al., 2013; Edmonds et al., 2001; Vivo-Vilches et al., 2018). Therefore, ^{129}I may provide a chronological marker for ISOW spreading pathways in the eastern SPNA. The East Greenland Current (EGC) also carries large amounts of ^{129}I in near-surface to intermediate waters (Alfimov et al., 2004).

10 Similar to ^{129}I, the presence of Uranium-236 (^{236}U) in the Arctic and Atlantic Oceans is largely dominated by releases from European NRPs, but in contrast to ^{129}I, there is a significant component from GF (Casacuberta et al., 2014, 2016; Winkler et al., 2012). The ^{236}U/^{238}U atom ratio in surface waters of the North Sea was between $\sim 1000 \times 10^{-12}$ and $20,000 \times 10^{-12}$ in 2009 - 2010 due to the large influence from the NRPs (Christl et al., 2015a; 2017). In 2011 - 2012, the ^{236}U/^{238}U ratio in the Arctic Ocean ranged between $\sim 5 \times 10^{-12}$ in the very deep basins up to 3800×10^{-12} in AW influenced by releases from European

15 NRPs and/or potentially unconstrained inputs from Arctic Rivers (Casacuberta et al., 2016; in prep.). The ^{236}U/^{238}U ratios were comparably smaller (($40 - 1500$) $\times 10^{-12}$) along a section crossing the western North Atlantic from the Irminger Sea down to the Equator in 2010 (Casacuberta et al., 2014; Christl et al., 2012). Yet, LSW and DSOW were clearly identified by ^{236}U/^{238}U $> 1000 \times 10^{-12}$ (Casacuberta et al., 2014). In addition, the combination of both conservative tracers as the ^{129}I/^{238}U atom ratio provides a new tool to distinguish sources of these artificial tracers, which are characteristic of each sources, varying between

20 ^{129}I/^{238}U < 1 for GF to about 1 - 350 for European NRPs (Casacuberta et al., 2016; Christl et al., 2015b). The information on the source is important to identify circulation features as, for example, the exchange between the Nordic Seas and the Arctic Ocean (Casacuberta et al., in prep.; Wefing et al., in prep.). Thus, new measurements of both ^{129}I and ^{236}U should help better understanding the origin and mixing of water masses in the SPNA.

25 In this study, we present the distribution of ^{129}I and ^{236}U along the GEOVIDE transect (GEOTRACES GA01) from Portugal to Newfoundland in spring 2014. The ^{129}I concentrations are used alone or in combination with ^{236}U to investigate the influence from anthropogenic sources and to infer the composition, origin and spreading pathways of water masses in the SPNA. Finally, the 2014 data are compared to earlier ^{129}I observations to estimate circulation timescales of AWs tagged with reprocessing ^{129}I into the Labrador Sea.

2 Materials and methods

2.1 The cruise, study area and sample collection

The GEOVIDE cruise (Figure 1) covered the OVIDE line from Lisbon (Portugal) to the southern tip of Greenland (Cape Farewell), and from Cape Farewell to St. John's (Newfoundland, Canada) onboard the French *R/V Pourquoi pas?* between

5   May 15th and June 30th, 2014. This cruise is part of the GEOTRACES program (section GA01: http://www.geotraces.org/cruises/cruise-summary) and contributes from a geochemical perspective to the decade-long biannual sampling (2002 to 2016) of the OVIDE line (http://www.umr-lops.fr/Projets/Projets-actifs/OVIDE).

The water mass structure during GEOVIDE was assessed using an extended Optimum Multi-Parameter analysis (OMP) by

10   García-Ibáñez et al. (2018). The water masses dominating the upper water column were Central Waters represented by the East North Atlantic Central Water (ENACW), and SPMW, while LSW was the most abundant water mass at intermediate depths. Deeper parts were filled, from west to east, by DSOW, ISOW and North East Atlantic Deep Water lower (NEADW$_L$). Prior studies have shown that some of these water masses may contain artificial radionuclides discharged from European NRPs (e.g., Smith et al. 2005). From the North Sea, most nuclear reprocessing effluents are carried poleward by the Norwegian

15   Coastal Current (NCC) into the Nordic Seas (Edmonds et al., 1998; Raisbeck and Yiou, 2002) while mixing with the Norwegian Atlantic Current (NwAC) (Gascard et al., 2004; Kershaw and Baxter, 1995). The plume splits north of Norway, one branch enters the Barents Sea as Barents Sea Branch Water (BSBW) and the other branch approaches the Fram Strait west of Spitsbergen where it bifurcates again. One branch joins the EGC and recirculates southwards as Return Atlantic Water (RAW) (Fogelqvist et al., 2003) mixing with PIW, modified AW that has recirculated in the Arctic Ocean (Rudels et al.,

20   1999b) and IrSPMW. The West Spitsbergen Current (WSC) transports the remaining AW at shallow to intermediate depths into the Arctic Ocean via the Fram Strait Branch Water, where they recirculate in the Arctic Eurasian Basin before outflowing through the Fram Strait and continuing south carried by the EGC (Rudels, 2015).

This study is based on data of ^{129}I and ^{236}U determined in about 150 seawater samples collected from 14 depth profiles (Figure

25   1) using a rosette equipped with conductivity-temperature-depth sensors and 24 12L Niskin bottles. Sampling depths were chosen to collect water from the main water masses and circulation features at each station by considering conductivity, temperature and oxygen profiles. From east to west, depth profiles were located in the West European Basin (WEB: stations 1, 13, 21 and 26), the central Icelandic Basin (station 32), above the Reykjanes Ridge (station 38), the Irminger Sea (stations 44 and 60), the Labrador Sea (stations 64, 69 and 77), and on the shelf/slope of Greenland (stations 53 and 61) and Canada

30   (station 78). Additional surface samples were obtained using a 'FISH' device that allowed the collection of seawater from about 2 m depth at 8 locations placed between depth profiles. Samples for ^{129}I of ~ 0.5 L each were collected in dark plastic bottles and sealed with parafilm. The ^{236}U samples of 5 - 7 L each were collected in plastic cubitainers. Bottles and cubitainers were rinsed 3 times with seawater before sample collection to avoid potential contamination.

2.2 Iodine-129 purification and AMS measurement

The radiochemistry of [129]I was done following the method described in Michel et al. (2012) in the laboratory at EAWAG. About 300 - 450 mL of sample was spiked with ~ 1.5 mg of Woodward stable iodine ([127]I) carrier. All iodine was oxidized to

5   iodate adding 2 % $Ca(ClO)_2$, then reduced to iodide using $Na_2S_2O_5$ and 1 M $NH_3O \cdot HCl$. The purification of iodine was carried out using columns filled with DOWEX® 1×8 ion exchange resin. The column was conditioned with deionized water and diluted KNO_3 solution before the elution of iodine with 2.25 M KNO_3 solution. The iodine was precipitated as AgI by adding $AgNO_3$, then mixed with 4 - 5 mg of Ag and pressed into AMS cathodes. The compact 0.5 MV Tandy AMS system at ETH-Zurich was used to measure the [129]I/[127]I atom ratios (Vockenhuber et al., 2015). The [129]I/[127]I ratios were normalized with the

10   ETH-Zurich in-house standard D22 with a nominal [129]I/[127]I value of $(50.35 \pm 0.16) \times 10^{-12}$ (Christl et al., 2013b). Radiochemistry blanks (n = 24) were prepared with deionized water and processed together with seawater samples following the same analytical procedures. These blanks presented [129]I/[127]I ratios of $(0.7 - 4) \times 10^{-13}$ corresponding to $(0.5 - 3) \times 10^6$ atoms of [129]I. The [129]I concentrations were calculated based on measured [129]I/[127]I ratio and the know amounts of [127]I carrier added to each sample. The detection limit of < 0.3 fg [129]I depended on the measured [129]I/[127]I ratio of the Woodward iodine carrier which

15   is typically at the order of ~ 10^{-13}.

2.3 Uranium-236 purification and AMS measurement

Each seawater sample (5 - 7 L) was weighed, acidified to pH below 2 using concentrated suprapure HNO_3 and spiked with ~ 3 pg of [233]U (IRMM - 051). The uranium was co-precipitated with iron hydroxides upon addition of ~ 200 mg of U-free Fe^{2+}

20   solution and concentrated suprapure NH_4OH by rising the pH to ~ 8. The iron precipitate was syphoned, evaporated to dryness and re-dissolved using 8 M HNO_3. The purification of uranium was carried out using UTEVA columns (Triskem). The eluate was co-precipitated with ~ 1 mg of the U-free Fe^{2+} solution and evaporated to dryness. All uranium was converted to oxide form by heating the iron precipitates to 650 ºC, then mixed with 2 - 3 mg of niobium and pressed into AMS cathodes. The compact 0.5 MV Tandy AMS system at ETH-Zurich was used to measure [233]U, [236]U and [238]U following Christl et al. (2013a).

25   The measured [236]U/[233]U and [236]U/[238]U ratios were normalized to the ZUTRI ETH-Zurich in-house standard with nominal values of $(4055 \pm 200) \times 10^{-12}$ and $(33170 \pm 830) \times 10^{-12}$, respectively (Christl et al., 2013a). Radiochemistry blanks (n = 19) were prepared onboard and in the land-based laboratory with deionized water and processed together with seawater samples following same analytical procedures. The blanks presented [236]U/[233]U ratios < 10^{-4}, corresponding to < 40 ag of [236]U. The compact TANDY AMS system has an abundance mass sensitivity of ~ 10^{-12} for the mass range of actinides, corresponding to

30   an instrumental background level at the order of [236]U/[238]U ~ 10^{-14}. Due to a mistake in the laboratory, a total of 34 samples were accidentally cross-contaminated with a very high [236]U standard and therefore had to be background corrected for cross

talk. The uncertainty of this additional background correction led to higher errors reported for those samples (marked with '*' in Table 2).

3 Results and discussion

3.1 Concentrations of ^{129}I, atom ratios of ^{236}U/^{238}U and ^{129}I/^{236}U, and their relationship with water masses in 2014

5   The concentrations of ^{129}I and ^{236}U, and atom ratios of ^{236}U/^{238}U and ^{129}I/^{236}U are reported in Table 2. Detailed depth profiles for these radionuclides are displayed along with salinity, potential temperature and dissolved oxygen in the Supporting Information (Figure S1). The ^{129}I concentrations range from $(0.20 \pm 0.20) \times 10^7$ to $(256 \pm 4) \times 10^7$ at/kg. The ^{236}U/^{238}U ratios range from $(40 \pm 20) \times 10^{-12}$ to $(2350 \pm 370) \times 10^{-12}$. The ^{129}I/^{236}U ratios range from 0.50 ± 0.50 to 200 ± 60.

10   The results from this study are best described in relation to the water mass structure reported by García-Ibáñez et al., (2018), which has been represented with overlaid isohalines on the radionuclide distribution plots (Figure 2). The ^{129}I concentrations (Figure 2A) and ^{236}U/^{238}U ratios (Figure 2B) are generally higher west of ~ 25 °W in southward flowing waters than in northward flowing, low-latitude waters dominating the eastern SPNA. The highest ^{129}I concentrations (~ 250×10^7 at/kg) and ^{236}U/^{238}U ratios (~ 2350×10^{-12}) are present in PIW and RAW carried by the EGC and Labrador Current (LC) along the slopes

15   of Greenland and Canada. This water admixture can mix with DSOW precursor waters through winter convection in the Greenland Sea (e.g. Gascard et al., 2002) or directly intrude DSOW by cascading in the Labrador Sea (e.g. Falina et al., 2012). Consequently, the DSOW core, found at the deepest 100 m in the Irminger and Labrador Seas, presents ^{129}I concentrations in the $(85 - 100) \times 10^7$ at/kg range and ^{236}U/^{238}U ratios of $(1300 - 2300) \times 10^{-12}$, which is in agreement with high radionuclide levels reported for DSOW in earlier studies (Casacuberta et al., 2014; Orre et al., 2010; Smith et al., 2005, 2016). Intermediate

20   ^{129}I concentrations $((5 - 50) \times 10^7$ at/kg) and ^{236}U/^{238}U ratios $((500 - 1500) \times 10^{-12})$ characterize the water masses filling most of the remaining GEOVIDE section. In the upper 500 m, ENACWs record rather uniform ^{129}I concentrations (~ 10×10^7 at/kg) and ^{236}U/^{238}U ratios (~ 1000×10^{-12}) in the WEB (stations 1 to 21). ENACWs are carried by the NAC from subtropical latitudes to the eastern SPNA, where they transform into SPMW (McCartney and Talley, 1982). SPMWs nearly double ^{129}I concentrations of ENACW (^{236}U/^{238}U ratios are similar) and are the most abundant water mass in the upper water column

25   comprised between Greenland and the Subarctic Front (SAF; roughly at 22.5 °W, station 26). Subarctic Intermediate Water (SAIW) entrains SPMWs and ENACWs leading to ^{129}I concentrations of ~ 20×10^7 at/kg at stations 26 and 32. SAIW probably incorporates ^{129}I from precursor water masses (e.g., waters carried by LC and/or LSW) while forming in the western SPNA (Arhan, 1990). The 500–2000 m layer is dominated by LSW, which is produced by winter convection of SPMWs in the Labrador and Irminger Seas (e.g., Jong and Steur, 2016). LSW then spreads equatorward (e.g. Bersch et al., 2007) and

30   eastwards along the Icelandic Basin up to the WEB while mixing with surrounding waters of varying age and radionuclide content. Consequently, LSW displays a wide range of ^{129}I concentrations $((5 - 50) \times 10^7$ at/kg) and ^{236}U/^{238}U ratios $((700 -$

1250) $\times 10^{-12}$) decreasing downstream from its formation region. Similar depths are also influenced by Mediterranean Water (MW) with ^{129}I concentrations of ~ 3×10^7 at/kg, ^{236}U/^{238}U ratios of ~ 1000×10^{-12} and a mass contribution up to 70 % in the WEB (García-Ibáñez et al., 2018). In 2013, MW recorded average ^{129}I concentrations of 9×10^7 at/kg, andc~ 1600×10^{-12} for ^{236}U/^{238}U ratios at the outflow region in the Strait of Gibraltar (Castrillejo et al., 2017). Thus, 2014 data probably reflects the

5   dilution with old LSW and SPMW carrying less ^{129}I and ^{236}U than MW. Deeper parts of the section west of 20 °W and below 2000 m are influenced by ISOW, which is characterized by relatively high ^{129}I concentrations (($10 - 70$) $\times 10^7$ at/kg) and ^{236}U/^{238}U ratios (($900 - 1700$) $\times 10^{-12}$). ISOW is produced by mixing of old Norwegian Sea waters which receive direct radionuclide inputs from European RPs yet in lower amounts than for DSOW (Smith et al., 2005). After overflowing the Iceland–Scotland Sill, ISOW flows southwest through the Icelandic Basin into the Irminger and Labrador Seas filling depths

10   between LSW and DSOW (García-Ibáñez et al., 2018). ISOW may also enter the eastern SPNA entraining SPMW and LSW to form NEADW (e.g., van Aken and De Boer, 1995). The lowest ^{129}I concentrations (($0.2 - 2.0$) $\times 10^7$ at/kg) and ^{236}U/^{238}U ratios (($40 - 350$) $\times 10^{-12}$) are found at depths greater than 2000 m in the WEB are associated with NEADW$_L$.

The ^{129}I/^{236}U distribution is notably driven by the ^{129}I concentrations, which display a greater range (3 orders of magnitude)

15   than the ^{236}U/^{238}U ratios (2 orders of magnitude). Thus, the ^{129}I/^{236}U ratios are particularly high (> 20) in the western part of the section and particularly crontrasted in the Irminger and Labrador Seas (Figure 2C). The highest ^{129}I/^{236}U ratios (> 100) are present in waters transported by the shallow EGC and LC. Overflow waters are also distinguishable by their relatively high ^{129}I/^{236}U ratios (60 to 110 for DSOW, 15 to 40 for ISOW).

20   **3.2 Sources of ^{129}I and ^{236}U in the SPNA**

All samples show ^{129}I concentrations and ^{236}U/^{238}U ratios well above their natural values (~ 0.04×10^7 at·kg^{-1} for ^{129}I (Snyder et al., 2010) and $10^{-14} - 10^{-13}$ for ^{236}U/^{238}U atom ratios (Christl et al., 2012; Steier et al., 2008)), named here as the lithogenic background (LB). This had been also shown in previous studies, highlighting the influence of GF and NRPs on the presence of ^{129}I (e.g. Edmonds et al., 2001) and ^{236}U (Casacuberta et al., 2014; Christl et al., 2012) in the North Atlantic. As done in

25   earlier studies (Casacuberta et al., 2016; Christl et al., 2015b), we can estimate the contribution to our samples from those radionuclide sources by combining the ^{129}I/^{236}U and ^{236}U/^{238}U ratios in a binary mixing model (Figure 3). This simple model considers one temporarily constant endmember for each source (LB, GF, NRP) and addresses all possible binary mixing scenarios. Each sample is represented by one data point collected at a certain station (Figure 3A) or for a dominant water mass (Figure 3B to 3F) inferred from OMP analyses (García-Ibáñez et al., 2018). Most samples fall along the GF-NRP binary mixing

30   line with contributions from NRPs > 1 %. The highest NRP contribution, above 5 %, is associated notably with PIW, DSOW and to less extend with ISOW and newly formed LSW. Samples plotting closer to the GF endmember with contributions from NRP < 1 % were collected at easternmost stations (1 to 21) and correspond to: i) waters diluted with older waters carrying

notably GF (e.g., old LSW); ii) NEACW$_L$ that have no clear influence from European NRPs while flowing from subtropical latitudes to the SPNA. At least 6 samples separate from the GF - NRP mixing line and plot towards the LB endmember. These are associated with NEADW$_L$, which mixes with northward flowing Antarctic Bottom Water (van Aken and Becker, 1996), the oldest water mass in the SPNA (not exposed to the surface or atmosphere for decades) having little or no influence from

5   nuclear activities.

3.3 Evolution of ^{129}I in the SPNA

A described above, our results show that overflow waters transport significant amounts of artificial ^{129}I and ^{236}U particularly to the deep Labrador and Irminger Seas. In the case of ^{129}I, this had been documented (Figure 4) in previous studies that

10   composed an extensive time series (1993 – 2013) of ^{129}I concentrations for the central Labrador Sea (Edmonds et al., 2001; Orre et al., 2010; Smith et al., 2005, 2016). The correspondingc^{236}U/^{238}U ratios from 2014 are in the range of those reported for DSOW waters sampled at the Denmark Strait in 2010 (Casacuberta et al., 2014), yet further comparison is not yet possible due to the limited data on the novel ^{236}U tracer. In all the above ^{129}I studies, a rise in its concentrations due to the increased ^{129}I discharge rate from European NRPs was observed in the whole water column, being more pronounced (about 10 times

15   increase) in overflow waters (Figure 4A). The depth distribution of ^{129}I concentrations in the Labrador Sea in 2014 (station 69), displays ^{129}I concentrations in DSOW about 15 % lower than in 2012 – 2013 (Smith et al., 2016), yet the general shape of the depth profile is comparable (Figure 4A). The main difference between the ^{129}I depth profiles in the Irminger Sea (station 44) and central Labrador Sea (station 69) in 2014 is the surface ^{129}I peak in the latter one (Figure 4A), which is probably caused by waters that split off from the boundary currents, either the West Greenland Current or the LC. A similar assessment of ^{129}I

20   concentrations is now possible for the water column above the Reykjanes Ridge (station 38) and the Icelandic Basin (station 32) (Figure 4B), which was first studied in 1993 (Edmonds et al., 2001). The ^{129}I concentrations in the water column are 5 - 7 times higher in 2014 than in 1993. The most pronounced increase occurs in the upper 1000 m and in the deep Icelandic Basin dominated by SPMW and ISOW, respectively. The depth profiles of ^{129}I concentration measured in the WEB in 2014 (particularly station 21) resemble the one sampled at Porcupine Abyssal Plain (PAP) in 2012 by Vivo-Vilches et al. (2018)

25   (Figure 4C). The ^{129}I distribution in the upper 1000 m at PAP looks very similar to station 21 located 365 km northeast, and below that depth ^{129}I concentrations indicate and offset of less than 2.5×10^7 at/kg between the two depth profiles. This similarity suggests little time variation and similar water mass composition for that region, although PAP might present slightly larger ^{129}I concentrations because of its proximity to Sellafield and La Hague.

3.4 Tracing water mass circulation in the SPNA using ^{129}I and ^{236}U

We use the above information on the distributions, sources and time evolution of ^{129}I and ^{236}U to investigate the circulation of nuclear reprocessing effluents and in return, provide more insight on composition, spreading pathways and transport time scales of water masses in the SPNA.

3.4.1 Shallow water circulation in the eastern SPNA

Concentrations of ^{129}I that are more than one order of magnitude above the GF level (2.5×10^7 at/kg; Edmonds et al., 1998) have been reported in the upper eastern SPNA by earlier studies (e.g., He et al., 2013b), and in this study along with ^{129}I/^{236}U ratios > 1 for ENACWs that must have originated from the releases from Sellafield and La Hague NRPs. Thus, despite most

10   effluents flow northward from the North Sea, it seems that part of reprocessing ^{129}I (and ^{236}U) may enter directly the SPNA without previous recirculation in the Nordic Seas. It has been suggested that the outflow through the English Channel and the Irish Sea may lead to increase the ^{129}I concentrations in surface waters to levels above 20×10^7 at/kg and modify the isotopic iodine composition in the Bay of Biscay (He et al., 2013b). If that was the case, the different NAC branches could mix ENACW with reprocessing-labeled local waters and be transported southward by shallow currents (e.g. Lambelet et al., 2015;

15   Lherminier et al., 2010; Ríos et al., 1992). Indeed, NAC branches west of station 21 recirculated anti-cyclonically into the WEB bringing waters south across the OVIDE line in 2014 (Zunino et al., 2017). Further transformation of ENACW into SPMW results in ^{129}I concentrations two times higher in the Icelandic Basin than in the WEB (Figures 4B and 4C). This suggests near-surface transport of ^{129}I from European NRPs also across Iceland-Scotland into the eastern SPNA. Indeed, surface ^{129}I concentrations (Figure S2) increased up to 10^8 - 10^9 at/kg range in the Icelandic Basin and northwest of the British

20   Isles by 2010–2012 (Gómez-Guzmán et al., 2013; Vivo-Vilches et al., 2018). Thus, one could potentially use ^{129}I to trace ENACWs in the upper water column of the WEB and their transformation into SPMW. This is not clearly supported by ^{236}U levels (~ 10×10^6 at/kg) which are close to GF in the shallow eastern SPNA, yet European NRPs introduced at least 30 times less ^{236}U than ^{129}I (Christl et al., 2015b).

25   #### 3.4.2 Shallow water transport and cascading in the Irminger Sea and Labrador Sea

The tracer levels are particularly high in shelf, slope and very deep waters that surround Greenland and Newfoundland (Figure 2) allowing to identify key circulation features such as the EGC/LC and the DWBC in the Labrador and Irminger Seas (Figure 1). At shallow depths, the EGC (stations 53 to 64) presents remarkably high ^{129}I concentrations (up to ~ 250×10^7 at/kg) and ^{129}I/^{236}U ratios (up to 200), while they are significantly lower in the LC (station 78) which is characterized by comparably

30   higher ^{236}U/^{238}U ratios (up to 2350×10^{-12}) (Figure 2). Such differences on the ^{129}I and ^{236}U composition of the two shallow boundary currents probably results from the mixing between water masses of Atlantic, Arctic and Pacific origin carrying more

or less GF and NRP effluents. For example, the EGC shows particularly high ^{129}I concentrations and ^{129}I/^{236}U ratios because it is carrying Arctic water of Atlantic origin (PIW-Atlantic) and RAW that have been largely influenced by NRP effluents. The LC presents more ^{236}U and less ^{129}I probably due to the supply of Arctic water of Pacific origin (PIW-Pacific) through the Nares Strait (Curry et al., 2014). This PIW-Pacific carries a small ^{129}I signal mainly from GF (Ellis and Smith, 1999; Smith et

5 al., 1998), while its ^{236}U/^{238}U ratios are likely > 2000 × 10^{-12} due to GF and unconstrained Arctic rivers inputs (Casacuberta et al., 2016).

Shelf waters carried by the EGC are thought to descend down the Greenland slope feeding the East Greenland Spill Jet and DSOW (von Appen et al., 2014; Falina et al., 2012; Harden et al., 2014; Koszalka and Haine, 2013; Pickart et al., 2005; Rudels

10 et al., 1999a). The GEOVIDE section shows a rise of ^{129}I concentrations at certain depths on the Greenland slope (e.g., station 60; Figure 2 and Figure S1), and particularly in bottom waters of the Irminger Sea (station 44), which are probably related to the cascading of ^{129}I-rich waters from the Greenland Shelf. This finding would be supported by OMP analyses which estimate up to 20 % of PIW in the DSOW realm (García-Ibáñez et al., 2018). Similar processes might be taking place in the Canadian shelf but with PIW-Pacific water cascading to the bottom of the Labrador Sea. This would explain the slightly higher ^{236}U/^{238}U

15 ratios near the Newfoundland Shelf (station 77; Figure 2 and Figure S1) compared to offshore waters in the Labrador Sea (e.g., station 69), as well as, the higher ^{236}U/^{238}U ratios and lower ^{129}I concentrations in the deep Labrador Sea (influenced by PIW-Pacific) compared to the Irminger Sea (influenced by PIW-Atlantic) (Figure 2).

3.4.3 Spreading pathways of ISOW in the eastern SPNA

20 The ^{129}I tracer may help validating present interpretations of ISOW spreading pathways in the SPNA which are largely based on model outputs or on limited observations (Fleischmann et al., 2001; LeBel et al., 2008; Xu et al., 2010; Zou et al., 2017). The ISOW is best distinguished by its relative ^{129}I concentration maxima (not observed for ^{236}U) and ^{129}I/^{236}U ratios of 15 - 40 that are significantly higher than in surrounding waters (e.g., LSW, NEADW$_L$). This is particularly visible for ^{129}I concentrations in deeper parts of the Icelandic Basin and the WEB (Figures 4B and 4C), where the presence of ISOW has also

25 been inferred from OMP analyses (García-Ibáñez et al., 2018). Further, in the next years one can expect a stronger ^{129}I signal associated with ISOW in the SPNA due to the releases from the NRPs. Indeed, the ^{129}I concentrations have increased from 7 × 10^7 at/kg to 63 × 10^7 at/kg at the Iceland–Scotland Sill from 1993 to 2012 (Alfimov et al., 2004; Edmonds et al., 2001; Vivo-Vilches et al., 2018). The overflow of ISOW through the Iceland-Scotland Sill has increasing implications for the deep ventilation of the SPNA and for the magnitude of the AMOC (García-Ibáñez et al., 2018). Thus, future time series of time-

30 varying ^{129}I concentrations at GEOVIDE stations and further upstream may also be used to investigate timescales of ventilation in the North Atlantic Ocean.

3.4.4 Transit times and dilution factors of reprocessing-labelled Atlantic Waters

The evolution of ^{129}I (and ^{236}U) in the SPNA is closely related to the effluents discharged from the two European NRPs. In particular, the extensive time series of ^{129}I concentrations in overflow waters in the central Labrador Sea (Figure 5A) allows

5   investigating the time evolution of ^{129}I concentrations in relation to its discharges. For this, we use the ^{129}I input function estimated at 60 °N in the northern North Sea (green dashed line, primary y axis) by Christl et al. (2015b), which mixes the signal of both NRPs in the North Sea and applies a time lag of 2 and 4 years for La Hague and Sellafield, respectively. We fit the ^{129}I input function to the observations by applying a time lag that accounts for the transport or transit time from 60 °N (North Sea) to the central Labrador Sea, and a dilution factor that represents the mixing between waters tagged with NRPs and

10   'pristine' AWs carried by the NAC. The ^{129}I front passing in 1990 – 1995 at 60 °N (green line) arrives 50 times more diluted to the central Labrador Sea about 6 years later causing a sharp increase in measured ^{129}I concentrations (Figure 5A, blue fit). Such finding was first noticed by Smith et al. (2005), who estimated a similar ^{129}I input function using a different approach (transfer factors). In their work, they also found that ^{129}I measurements were about 30 % lower than estimated for the 2003 – 2009 period, possibly due to the weakening of the subpolar gyre. In 2012 – 2013, the measured ^{129}I concentrations increased

15   again (~ 200 %) very likely due to the delayed arrival of the same 1990s ^{129}I front, but that was transported north through the Fram Strait into the Nansen Basin, where the plume recirculated prior to returning with the EGC to the Nordic Seas (Smith et al., 2011). Data reported in this study (2014) supports this 'Arctic loop' and suggests that the second ^{129}I front probably peaked before the GEOVIDE cruise. Indeed, the second ^{129}I peak is best fitted by diluting the reprocessing signal about 30 times and assuming a transit time of about 14 years (red line) from 60 °N. This would be in line with the current understanding (Orre et

20   al., 2010; Smith et al., 2005, 2011, 2016) that AWs labelled with reprocessing effluents follow at least two paths before arriving to the Labrador Sea: i) one short path into the Nordic Sea and then to the SPNA that takes approximately 8 - 10 years from the NRPs, and ii) a long path which adds approximately 8-years more of recirculation in the Arctic Ocean resulting in 16 - 18 years of transit time from the NRPs to the Labrador Sea. A similar exercise for ^{236}U (Figure 6B) shows that the single ^{236}U measurement available for overflow waters in the central Labrador Sea (2014, this work) is above the concentrations predicted

25   using the two fits. Thus, ^{236}U data would agree with the hypothesis of a delayed, second ^{129}I pulse, yet more observations are needed to confirm this by means of ^{236}U. Note that the latter input function for the Labrador Sea (Figure 5, red line) only provides an upper estimate for ^{129}I transit times, which in reality should fall between 8 and 18 years.

4 Conclusions

30   The distribution of artificial ^{129}I and ^{236}U in the SPNA was governed by the main water mass circulation in spring 2014. The highest ^{129}I concentrations and $^{236}U/^{238}U$ ratios are associated with water masses originating from the Nordic Seas (DSOW,

ISOW) or the Arctic Ocean (PIW), while at the other end, ENACW and NEADW$_L$ transported from low latitudes north into the SPNA present ^{129}I concentrations and ^{236}U/^{238}U ratios of about 2 – 3 orders of magnitude lower. The ^{236}U/^{238}U - ^{129}I/^{236}U dual tracer approach indicates that all water masses, except deepest NEADW$_L$, are influenced by GF and NRPs. ENACW is also influenced by effluents from NRPs, which suggests that part of the radioactive releases split off from the mainstream and

5   enter the eastern SPNA either through direct exchange at the English Channel/Irish Sea or at the passage between Iceland and Scotland. Other key circulation features such as the shallow transport of PIW and RAW by the EGC and LC, or the deep North Atlantic ventilation by overflow waters (DSOW, ISOW) are particularly visible thanks to the presence of reprocessing ^{129}I and ^{236}U. For example, ISOW is tagged with relatively high ^{129}I and, therefore, it can be traced while spreading eastwards into the WEB. The combination of ^{236}U/^{238}U and ^{129}I/^{236}U allows differentiating water mass composition and origin. For example, the

10   LC appears to receive shallow PIW-Pacific through the Canadian Archipelago, while the EGC would carry RAW and PIW-Atlantic. The RAW/PIW-Atlantic and PIW-Pacific appear to cascade and contribute to overflow water (DSOW) in the Irminger and Labrador Seas, respectively. This work contributes new ^{129}I data, extending the existing time series in the Labrador Sea/Irminger Sea and allowing a first assessment of time-varying ^{129}I concentrations east of Reykjanes Ridge. Increasing ^{129}I concentrations are observed in the western part of the GEOVIDE section and in the Icelandic Basin, although

15   the short observation time (2012 – 2014) does not allow yet seeing temporal trends of ^{129}I levels in the WEB. The ^{129}I data in overflow waters of the central Labrador Sea (1993 – 2014) can be fitted with reprocessing ^{129}I (and ^{236}U) input functions to better understand the transport time scales and dilution factors of waters tagged by the NRP signal. Results show that water circulation transit times from the NRPs to the deep Labrador Sea probably fall between the maximum of 16 – 8 years (including recirculation in the Arctic Eurasian Basin) and the shorter loop trough the Nordic Seas of 8 - 10 years. Longer time series of

20   ^{129}I and ^{236}U will allow confirming some of these findings relevant for the understanding of the AMOC and calibrate circulation models. Thus, these tracers may provide new information on the circulation and mixing processes of waters masses involved in the changing AMOC.

Acknowledgements

We are grateful to the captain and crew of *R/V Pourquoi Pas?*, as well as the technical team for their work at sea (P. Branellec,
25   F. Desprez de Gésincourt, M. Hamon, C. Kermabon, P. Le Bot, S. Leizour, O. Ménage, F. Pérault, and E. de Saint-Léger). A big thank to Yi Tang for help sampling and to Anita Schlatter for assistance in the laboratory. Thanks to J.-L. Menzel and the group of E. Achterberg (GEOMAR, Kiel) for providing the FISH device to collect surface seawater. The work of C. Schmechtig with the LEFE-CYBER database management is also acknowledged. Some of the ^{129}I data discussed from the literature were kindly provided by V. Alfimov, H. Edmonds and J. N. Smith. Several figures were created using *Ocean Data
30   View* (Schlitzer, 2017). We would also like to thank Natalie Dubois and Alfred Lück for providing the laboratory space and assistance at EAWAG. The GEOVIDE cruise was funded by the French National Research Agency (ANR-13-BS06-0014, ANR-12-PDOC-0025-01), the French National Center for Scientific Research (CNRS-LEFE-CYBER), the LabexMER (ANR-

10-LABX-19), and Ifremer. This work was funded by the Ministerio de Economía y Competitividad of Spain (MDM2015-0552), the Generalitat de Catalunya (MERS 2017 SGR-1588) and consortium partners of the ETH-Zurich Laboratory of Ion Beam Physics (EAWAG, EMPA, and PSI). M. Castrillejo was funded by a FPU PhD studentship (AP-2012-2901) from the Ministerio de Educación, Cultura y Deporte of Spain and the ETH Zurich Postdoctoral Fellowship Program (17-2 FEL-30), co-funded by the Marie Curie Actions for People COFUND Program. N. Casacuberta's research was funded by the AMBIZIONE grant (PZ00P2_154805) from the Swiss National Science Foundation. M.I. García-Ibáñez was supported by the Spanish Ministry of Economy and Competitiveness through the BOCATS (CTM2013-41048-P) project co-funded by the Fondo Europeo de Desarrollo Regional 2014–2020 (FEDER).

References

Aarkrog, A., Boelskifte, S., Dahlgard, H., Duniec, S., Hallstadius, L., Holm, E. and Smith, J. N.: Technetium-99 and Cesium-134 as long distance tracers in Arctic Waters, Estuar. Coast. Shelf Sci., 24, 637–647, 1987.

Aarkrog, A., Dahlgaard, H., Hallstadius, L., Hansen, H. and Holm, E.: Radiocaesium from Sellafield effluents in Greenland waters, Nature, 304, 49–51, 1983.

Alfimov, V., Aldahan, A. and Possnert, G.: Water masses and ^{129}I distribution in the Nordic Seas, Nucl. Inst. Methods Phys. Res. B, 294, 542–546, doi:10.1016/j.nimb.2012.07.042, 2013.

Alfimov, V., Aldahan, A., Possnert, G. and Winsor, P.: Tracing water masses with ^{129}I in the western Nordic Seas in early Spring 2002, Geophys. Res. Lett., 31, L19305, 2004.

Arhan, M. The North Atlantic Current and the subarctic intermediate water, J. Mar. Res., 48(1), 109–144, 1990.

Beasley, T., Cooper, L. W., Grebmeier, J. M., Aagaard, K., Kelley, J. M. and Kilius, L. R.: ^{237}Np/^{129}I Atom Ratios in the Arctic Ocean: Has ^{237}Np from Western European and Russian Fuel Reprocessing Facilities Entered the Arctic Ocean ?, J. Environ. Radioact., 39(3), 255–277, 1998.

Bersch, M., Yashayaev, I. and Koltermann, K. P.: Recent changes of the thermohaline circulation in the subpolar North Atlantic, Ocean dy, 57, 223–235, doi:10.1007/s10236-007-0104-7, 2007.

Casacuberta, N., Christl, M., Lachner, J., van der Loeff, M. R., Masqué, P. and Synal, H.-A.: A first transect of ^{236}U in the North Atlantic Ocean, Geochim. Cosmochim. Acta, 133, 34–46, doi:10.1016/j.gca.2014.02.012, 2014.

Casacuberta, N., Christl, M., Vockenhuber, C., Wefing, A.-M., Wacker, L., Masqué, P., Synal, H.-A. and Rutgers van der Loeff, M.: Tracing Atlantic Water s intro the Arctic Ocean by means of ^{129}I and ^{236}U, in prep..

Casacuberta, N., Masqué, P., Henderson, G., Rutgers van-der-Loeff, M., Bauch, D., Vockenhuber, C., Daraoui, a., Walther, C., Synal, H. -a. and Christl, M.: First ^{236}U data from the Arctic Ocean and use of ^{236}U/^{238}U and ^{129}I/^{236}U as a new dual tracer, Earth Planet. Sci. Lett., 440, 127–134, doi:10.1016/j.epsl.2016.02.020, 2016.

Castrillejo, M., Casacuberta, N., Christl, M., Garcia - Orellana, J., Vockenhuber, C., Synal, H.-A. and Masqué, P.:

Anthropogenic ^{236}U and ^{129}I in the Mediterranean Sea: First comprehensive distribution and constrain of their sources, Sci. Total Environ., 593–594, 745–759, doi:10.1016/j.scitotenv.2017.03.201, 2017.

Christl, M., Casacuberta, N., Lachner, J., Herrmann, J. and Synal, H. A.: Anthropogenic ^{236}U in the North Sea - A Closer Look into a Source Region, Env. Sci. and Tech., 2017.

5   Christl, M., Casacuberta, N., Lachner, J., Maxeiner, S., Vockenhuber, C., Synal, H. A., Goroncy, I., Herrmann, J., Daraoui, A., Walther, C. and Michel, R.: Status of ^{236}U analyses at ETH Zurich and the distribution of ^{236}U and ^{129}I in the North Sea in 2009, Nucl. Instruments Methods Phys. Res. Sect. B Beam Interact. with Mater. Atoms, 361, 510–516, doi:10.1016/j.nimb.2015.01.005, 2015a.

Christl, M., Casacuberta, N., Vockenhuber, C., Elsässer, C., Bailly du Bois, P., Herrmann, J. jürgen and Synal, H.-A.:

10   Reconstruction of the ^{236}U input function for the Northeast Atlantic Ocean: Implications for ^{129}I/^{236}U and ^{236}U/^{238}U-based tracer ages, J. Geophys. Res. Ocean., 1–16, doi:10.1002/2014JC010472.Received, 2015b.

Christl, M., Lachner, J., Vockenhuber, C., Goroncy, I., Herrmann, J. and Synal, H. A.: First data of Uranium-236 in the North Sea, Nucl. Instruments Methods Phys. Res. Sect. B Beam Interact. with Mater. Atoms, 294, 530–536, doi:10.1016/j.nimb.2012.07.043, 2013a.

15   Christl, M., Lachner, J., Vockenhuber, C., Lechtenfeld, O., Stimac, I., van der Loeff, M. R. and Synal, H.-A.: A depth profile of uranium-236 in the Atlantic Ocean, Geochim. Cosmochim. Acta, 77, 98–107, doi:10.1016/j.gca.2011.11.009, 2012.

Christl, M., Vockenhuber, C., Kubik, P. W., Wacker, L., Lachner, J., Alfimov, V. and Synal, H.: The ETH Zurich AMS facilities : Performance parameters and reference materials, Nucl. Inst. Methods Phys. Res. B, 294, 29–38, doi:10.1016/j.nimb.2012.03.004, 2013b.

20   Curry, B., Lee, C. M., Petrie, B., Moritz, R. E. and Kwok, R.: Multiyear Volume, Liquid Freshwater, and Sea Ice Transports through Davis Strait, 2004-10, J. Phys. Oceanogr., 44, 1244–1266, 2014.

Dahlgaard, H.: Transfer of European Coastal Pollution to the Arctic : Radioactive Tracers, Mar. Pollut. Bull., 31(95), 3–7, 1995.

Daniault, N., Mercier, H., Lherminier, P., Sarafanov, A., Falina, A., Zunino, P., Pérez, F. F., Ríos, A. F., Ferron, B., Huck, T.

25   and Thierry, V.: The northern North Atlantic Ocean mean circulation in the early 21st century, Prog. Oceanogr., 146 (June), 142–158, doi:10.1016/j.pocean.2016.06.007, 2016.

Doney, S. C. and Jenkins, W. J.: Ventilation of the deep western boundary current and abyssal western North Atlantic: Estimates from tritium and ^{3}He distributions, J. Phys. Oceanogr., 24, 638–659, 1994.

Edmonds, H. N., Smith, J. N., Livingston, H. D., Kilius, L. R. and Edmond, J. M.: ^{129}I in archived seawater samples, Deep.

30   Res. Part I Oceanogr. Res. Pap., 45, 1111–1125, doi:10.1016/S0967-0637(98)00007-7, 1998.

Edmonds, H. N., Zhou, Z. Q., Raisbeck, G. M., Yiou, F., Kilius, L. and Edmond, J. M.: Distribution and behavior of anthropogenic ^{129}I in water masses ventilating the North Atlantic Ocean, J. Geophys. Res., 106, 6881–6894, 2001.

Ellis, K. M. and Smith, J. N.: The flow of radionuclides through the Canadian Archipelago, Proc. IAEA Mainre Pollut. Symp. IAEA Tech. Doc., 1094, 462–464, Monaco, 1999.

Falina, A., Sarafanov, A., Mercier, H., Lherminier, P., Sokov, A. and Daniault, N.: On the cascading of dense shelf waters in the Irminger Sea, J. Phys. Oceanogr., 42, 2254–2267, 2012.

Fleischmann, U., Hildebrandt, H., Putzka, A. and Bayer, R.: Transport of newly ventilated deep water from the Iceland Basin to the West European Basin, Deep Sea Res., 48B, 1793–1819, 2001.

5 Fogelqvist, E. J., Blindheim, J., Tanhua, T. T., Osterhus, S., Buch, E. and Rey, F.: Greenland-Scotland overflow studied by hydro-chemical multivariate analysis, Deep Sea Res., Part I, 50, 73–102, 2003.

García-Ibáñez, M.-I., Pérez, F. F., Lherminier, P., Zunino, P. and Tréguer, P.: Water mass distributions and transports for the 2014 GEOVIDE curise in the North Atlantic, Biogeosciences, 15, 2075-2090, 2018.

Gascard, J. C., Raisbeck, G., Sequeira, S., Yiou, F. and Mork, K. A.: The Norwegian Atlantic Current in the Lofoten Basin

10 inferred from hydrological and tracer data (^{129}I) and its interaction with the Norwegian Coastal Current, Geophys. Res. Lett., 31, L01308, 2004.

Gascard, J., Watson, A. J., Messias, M.-J., Olsson, K. A., Johannessen, T. and Simonsen, K.: Long-lived vortices as a mode of deep ventilation in the Greenland Sea, Nature, 416(April), 525–527, 2002.

Gómez-guzmán, J. M., Villa, M., Le Moigne, F., López-gutiérrez, J. M. and García-león, M.: AMS measurements of ^{129}I in

15 seawater around Iceland and the Irminger Sea, Nucl. Inst. Methods Phys. Res. B, 294, 547–551, doi:10.1016/j.nimb.2012.07.045, 2013.

Hansen, B. and Osterhus, S.: North Atlantic - Nordic Sea exchanges, Prog. Oceanogr., 45, 109–208, 2000.

Harden, B. E., Pickart, R. S. and Benfrew, I. A.: Offshore Transport of Dense Water from the East Greenland Shelf, J. Phys. Oceanogr., 229–245, doi:10.1175/JPO-D-12-0218.1, 2014.

20 He, P., Aldahan, a., Possnert, G. and Hou, X. L.: A summary of global ^{129}I in marine waters, Nucl. Instruments Methods Phys. Res. Sect. B Beam Interact. with Mater. Atoms, 294, 537–541, doi:10.1016/j.nimb.2012.08.036, 2013a.

He, P., Hou, X., Aldahan, A., Possnert, G. and Yi, P.: Iodine isotopes species fingerprinting environmental conditions in surface water along the northeastern Atlantic Ocean., Sci. Rep., 3, 2685, doi:10.1038/srep02685, 2013b.

Holm, E., Persson, B. R. R., Hallstadius, L., Aarkrog, A. and Dahlgaard, H.: Radio-cesium and transuranium elements in the

25 Greenland and Barents Seas, Oceanol. Acta, 6, 457–462, 1983.

Jong, M. F. and Steur, L.: Strong winter cooling over the Irminger Sea in winter 2014–2015, exceptional deep convection, and the emergence of anomalously low SST, Geophy. Res. Lett., 43, 7106–7113, doi:10.1002/2016GL069596.Received, 2016.

Karcher, M., Smith, J. N., Kauker, F., Gerdes, R. and Smethie, W. M.: Recent changes in Arctic Ocean circulation revealed by iodine-129 observations and modeling, J. Geophys. Res. Ocean., 117, 1–17, doi:10.1029/2011JC007513, 2012.

30 Kershaw, P. and Baxter, A.: The transfer of reprocessing wastes from north-west Europe to the Arctic, Deep Sea Res., Part II, 42(6), 1413–1448, 1995.

Koszalka, I. M. and Haine, T. W. N.: Fates and Travel Times of Denmark Strait Overflow Water in the Irminger Basin, J. Phys. Oceanogr., December, 2611–2628, doi:10.1175/JPO-D-13-023.1, 2013.

Lambelet, M., van de Flierdt, T., Crocket, K., Rehkämper, M., Kreissig, K., Coles, B., Rijkenberg, M. J. a., Gerringa, L. J. a.,

de Baar, H. J. W. and Steinfeldt, R.: Neodymium isotopic composition and concentration in the western North Atlantic Ocean: results from the GEOTRACES GA02 section, Geochim. Cosmochim. Acta, 177, 1–29, doi:10.1016/j.gca.2015.12.019, 2016.

LeBel, D. A., Jr., Smethie, W. M., Rhein, M., Kieke, D., Fine, R. A., Bullister, J. L., D., M., Roether, W., Weiss, R. F., Andrié, C., Smythe-Wright, D. and E, J. P.: The formation rate of North Atlantic Deep Water and eighteen Degree water calculated from CFC-11 inventories observed during WOCE, Deep Sea Res. Part I Oceanogr. Res. Pap., 55(8), 891–910, 2008.

Lherminier, P., Mercier, H., Huck, T., Gourcuff, C., Perez, F. F., Morin, P., Sarafanov, A. and Falina, A.: The Atlantic Meridional Overturning Circulation and the subpolar gyre observed at the A25-OVIDE section in June 2002 and 2004, Deep Sea Res. Part I Oceanogr. Res. Pap., 57(11), 1374–1391, doi:10.1016/j.dsr.2010.07.009, 2010.

McCartney, M. and Talley, L. D.: The Subpolar Mode Water of the North Atlantic Ocean, J. Phys. Oceanogr., 12, 1169–1188, 1982.

Mercier, H., Lherminier, P., Sarafanov, A., Gaillard, F., Daniault, N., Desbruyères, D., Falina, A., Ferron, B., Gourcuff, C., Huck, T. and Thierry, V.: Variability of the meridional overturning circulation at the Greenland–Portugal OVIDE section from 1993 to 2010, Prog. Oceanogr., doi:10.1016/j.pocean.2013.11.001, 2013.

Michel, R., Daraoui, a., Gorny, M., Jakob, D., Sachse, R., Tosch, L., Nies, H., Goroncy, I., Herrmann, J., Synal, H. a., Stocker, M. and Alfimov, V.: Iodine-129 and iodine-127 in European seawaters and in precipitation from Northern Germany, Sci. Total Environ., 419, 151–169, doi:10.1016/j.scitotenv.2012.01.009, 2012.

Orre, S., Smith, J. N., Alfimov, V. and Bentsen, M.: Simulating transport of [129]I and idealized tracers in the northern North Atlantic Ocean, Environ. Fluid Mech., 10, 213–233, 2010.

Pérez, F. F., Mercier, H., Vázquez-rodríguez, M., Lherminier, P., Velo, A., Pardo, P. C., Rosón, G. and Ríos, A. F.: Atlantic Ocean CO_2 uptake reduced by weakening of the meridional overturning circulation, Nat. Geosci., 6 (February), doi:10.1038/ngeo1680, 2013.

Pickart, R. S., Torres, D. J. and Fratantoni, P. S.: The East Greenland Spill Jet, J. Phys. Oceanogr., 58 (Dietrich 1964), 1037–1053, 2005.

Raisbeck, G. M. and Yiou, F.: Use of [129]I as an oceanographic tracer in the Nordic Seas, Pap. Present. 5th Int. Conf. Environ. Radioact. Arct. Antarct. St. Petersburg, Russ., 127–130, 2002.

Raisbeck, G. M., Yiou, F., Zhou, Z. Q. and Kilius, L. R.: [129]I from nuclear fuel reprocessing facilities at Sellafield (U.K.) and La Hague (France); potential as an oceanographie tracer, J. Mar. Syst., 6(5–6), 561–570, doi:10.1016/0924-7963(95)00024-J, 1995.

Ríos, A. F., Pérez, F. F. and Fraga, F.: Water masses in the upper and middle North Atlantic Ocean east of the Azores, Deep Sea Res., 39 (3/4), 645–658, 1992.

Rudels, B.: Arctic Ocean circulation, processes and water masses: A description of observations and ideas with focus on the period prior to the International Polar Year 2007 – 2009, Prog. Oceanogr., 132, 22–67, doi:10.1016/j.pocean.2013.11.006, 2015.

Rudels, B., Eriksson, P., Gronvall, H., Hietala, R. and Launiainen, J.: Hydrographic Observations in Denmark Strait in Fall

1997, and their Implications for the Entrainment into the Overflow Plume, Geophys. Res. Lett., 26(9), 1325–1328, 1999a.

Rudels, B., Friedrich, H. J. and Quadfasel, D.: The Arctic Circumpolar Boundary Current, Deep Sea Res., Part II, 46, 1999b.

Schlitzer, R.: Ocean Data View, http://odv.awi.de, 2017.

Smith, J. N., Ellis, K. M. and Kilius, L. R.: [129]I and ^{137}Cs tracer measurements in the Arctic Ocean, Deep. Res. Part I Oceanogr.
5   Res. Pap., 45, 959–984, doi:10.1016/S0967-0637(97)00107-6, 1998.

Smith, J. N., Jones, E. P., Moran, S. B., Jr, W. M. S. and Kieser, W. E.: Iodine-129/CFC-11 transit times for Denmark Strait Overflow Water in the Labrador and Irminger Seas, J. Geophys. Res., 110, 1–16, doi:10.1029/2004JC002516, 2005.

Smith, J. N., Mclaughlin, F. A., Smethie Jr, W. M., Moran, S. B. and Lepore, K.: Iodine-129, ^{137}Cs, and CFC-11 tracer transit time distributions in the Arctic Ocean, J. Geophys. Res., 116, 1–19, doi:10.1029/2010JC006471, 2011.

10 Smith, J. N., Smethie Jr, W. M., Yashayev, I., Curry, R. and Aztsu-Scott, K.: Time series measurements of transient tracers and tracer-derived transport in the Deep Western Boundary Current between the Labrador Sea and the subtropical Atlantic Ocean at line W, J. Geophys. Res. Ocean., 121, 1–24, doi:10.1002/2016JC011759.Received, 2016.

Snyder, G., Aldahan, A. and Possnert, G.: Global distribution and long-term fate of anthropogenic I-129 in marine and surface water reservoirs, Geochemistry Geophys. Geosystems, 11, doi:10.1029/2009GC002910, 2010.

15 Steier, P., Bichler, M., Keith Fifield, L., Golser, R., Kutschera, W., Priller, A., Quinto, F., Richter, S., Srncik, M., Terrasi, P., Wacker, L., Wallner, A., Wallner, G., Wilcken, K. M. and Maria Wild, E.: Natural and anthropogenic [236]U in environmental samples, Nucl. Instruments Methods Phys. Res. Sect. B, 266(10), 2246–2250, doi:10.1016/j.nimb.2008.03.002, 2008.

Sy, A., Rhein, M., Lazier, J., Koltermann, K., Meincke, J., Putzka, A. and Bersch, M.: Surprisingly rapid spreading of newly formed intermediate waters across the North Atlantic Ocean, Nature, 386, 675–679, 1997.

20 Tanhua, T., Bulsiewicz, K. and Rhein, M.: Spreading of overflow water from the Greenland to the Labrador Sea, Geophys. Res. Lett., 32, L10605, 2005.

van Aken, H. M. and Becker, G.: Hydrography and through-flow in the northeastern North Atlantic Ocean: the NANSEN project, Prog. Oceanogr., 38(4), 297–346, 1996.

van Aken, H. M. and De Boer, C. J.: On the synoptic hydrography of intermediate and deep water masses in the Iceland Basin,
25 Deep Sea Res., Part I, 42(2), 1995.

Vivo-Vilches, C., López-Gutiérrez, J. M., Periáñez, R., Marcinko, C., Le Moigne, F., Mcginnity, P., Peruchena, J. I. and Villa-Alfageme, M.: Recent evolution of [129]I levels in the Nordic Seas and the North Atlantic Ocean, Sci. Total Environ., 621, 376–386, doi:10.1016/j.scitotenv.2017.11.268, 2018.

Vockenhuber, C., Casacuberta, N., Christl, M. and Synal, H. A.: Accelerator Mass Spectrometry of [129]I towards its lower
30 limits, Nucl. Instruments Methods Phys. Res. Sect. B, 361, 445–449, doi:10.1016/j.nimb.2015.01.061, 2015.

von Appen, W.-J., Koszalka, I. M., Pickart, R. S., Haine, T. W. N., Mastropole, D., Magaldi, M. G., Valdimarsson, H., Girton, J., Jochumsen, K. and Krahmann, G.: The East Greenland Spill Jet as an important component of the Atlantic Meridional Overturning Circulation, Deep Sea Res. Part I, 92, 75–84, 2014.

Wefing, A.-M., Casacuberta, N., Vockenhuber, C., Christl, M. and Rutgers van der Loeff, M.: Distribution of I-129 and U-

236 in the Fram Strait, in prep..

Winkler, S. R., Steier, P. and Carilli, J.: Bomb fall-out [236]U as a global oceanic tracer using an annually resolved coral core., Earth Planet. Sci. Lett., 359–360(1), 124–130, doi:10.1016/j.epsl.2012.10.004, 2012.

Xu, X., Schmitz Jr, W. J., Hurlburt, H. E., Hogan, P. J. and Chassignet, E. P.: Transport of Nordic Seas overflow water into
5   and within the Irminger Sea : An eddy - resolving simulation and observations, J. Geophys. Res., 115 (September), C12048, doi:10.1029/2010JC006351, 2010.

Zou, S., Lozier, S., Zenk, W., Bower, A. and Johns, W.: Observed and modeled pathways of the Iceland Scotland Over flow Water in the eastern North Atlantic, Prog. Oceanogr., 159 (April), 211–222, doi:10.1016/j.pocean.2017.10.003, 2017.

Zunino, P., Lherminier, P., Mercier, H., Daniault, N., García-Ibáñez, M.-I. and Pérez, F. F.: The GEOVIDE cruise in May -
10   June 2014 revealed an intense MOC over a cold and fresh subpolar North Atlantic, Biogeosciences, 14, 5323-5342, 2017.

30

Table 1. Acronyms used to define water masses, geographic locations and radionuclide sources.

Acronym	
AMOC	Atlantic Meridional Overturning Circulation
AMS	Accelerator Mass Spectrometry
AW	Atlantic Water
BSBW	Barents Sea Branch Water
DSOW	Denmark Strait Overflow Water
DWBC	Deep Western Boundary Current
EGC	East Greenland Current
ENACW	East North Atlantic Central Water
GF	Global Fallout
ISOW	Iceland-Scotland Overflow Water
LB	Lithogenic Background
LC	Labrador Current
LH	La Hague
LSW	Labrador Sea Water
MW	Mediterranean Water
NAC	North Atlantic Current
NCC	Norwegian Coastal Current
NEADW$_L$	North East Atlantic Deep Water lower
NRP	Nuclear Reprocessing Plant
NwAC	Norwegian Atlantic Current
OMP	Optimum Multi-Parameter analysis
PAP	Porcupine Abyssal Plain
PIW	Polar Intermediate Water
RAW	Return Atlantic Water
SAIW	Sub-Arctic Intermediate Water
SF	Sellafield
SPMW	Sub-Polar Mode Water
SPNA	Sub-Polar North Atlantic
WEB	West European Basin
WSC	West Spitsbergen Current

Table 2. Concentrations of ^{129}I and ^{236}U, and atom ratios of ^{236}U/^{238}U and ^{129}I/^{236}U in seawater samples collected during the GEOVIDE cruise in spring 2014. Uncertainties of radionuclide concentrations and the ^{236}U/^{238}U ratio are given as one sigma deviations. The uncertainty of the ^{129}I/^{236}U ratio was propagated from the concentration uncertainty. *^{236}U data corrected for cross talk contamination.

Station and location	ETH Code	Depth m	Dominant water mass	Salinity	Pot. Temp. °C	Oxygen μmol·kg⁻¹	^{129}I ×10⁷ at·kg⁻¹	^{236}U ×10⁶ at·kg⁻¹	^{236}U/^{238}U ×10⁻¹² at·at⁻¹	^{129}I/^{236}U at·at⁻¹
Station 1 40°19.99' N 10°2.16' W Bottom depth: 3536 m	TU1141-H160122	5	ENACW	35.16	16.49	250	7.2 ± 0.1	9.2 ± 0.4	1130 ± 60	7.9 ± 0.4
	TU1151-H160120	25	ENACW	35.50	15.09	262	7.4 ± 0.1	10.6 ± 0.8	1330 ± 100	7.0 ± 0.5
	TU1152-H160119	50	ENACW	35.70	13.76	254	8.2 ± 0.1	9.2 ± 0.5	1110 ± 60	8.9 ± 0.5
	TU1153-H160118	100	ENACW	35.74	13.03	239	8.3 ± 0.1	8.4 ± 0.4	1100 ± 50	9.9 ± 0.5
	TU1154-H160110	200	ENACW	35.71	12.50	228	7.5 ± 0.1	8.9 ± 0.5	1050 ± 60	8.5 ± 0.5
	TU1147-H160103	400	ENACW	35.65	11.63	212	6.6 ± 0.1	8.6 ± 0.5	1030 ± 70	7.7 ± 0.5
	TU1134-H160080	1000	MW	36.15	11.13	177	3.4 ± 0.1	8.3 ± 0.4	1000 ± 60	4.1 ± 0.2
	TU1135-H160079	1200	MW	36.11	10.42	182	3.1 ± 0.1	8.4 ± 0.4	990 ± 60	3.7 ± 0.2
	TU1136-H160078	1600	MW/LSW	35.52	6.74	220	3.1 ± 0.1	10.0 ± 0.6	1010 ± 60	3.1 ± 0.2
	TU1123-H160077	2000	LSW	35.09	4.07	248	2.1 ± 0.1	7.9 ± 0.4	940 ± 50	2.6 ± 0.1
	TU1124-H160076	2500	NEADW$_L$	35.00	3.16	246	1.0 ± 0.1	2.5 ± 0.6	340 ± 110	4.1 ± 0.9
	TU1125-H160075	3000	NEADW$_L$	34.95	2.60	244	0.2 ± 0.2	2.3 ± 0.3	270 ± 30	0.9 ± 0.9
	TU1126-H160074	3506	NEADW$_L$	34.92	2.28	243	0.2 ± 0.2	4.4 ± 0.3	540 ± 40	0.5 ± 0.5
Surface 1 40°19.98' N 9°27.57' W	TU1148-H160123	5	ENACW				7.0 ± 0.1	9.3 ± 0.4	1160 ± 50	7.5 ± 0.4
Station 13 41°2298' N 13°53.26' W Bottom depth: 5347 m	TU1155-H160211	10	ENACW	35.85	15.55	259	8.5 ± 0.3	8.5 ± 0.4	950 ± 40	10.0 ± 0.5
	TU1156-H160085	30	ENACW	35.83	15.00	259	7.7 ± 0.3	8.6 ± 0.3	980 ± 40	8.9 ± 0.5
	TU1158-H160061	65	ENACW	35.76	13.16	251	7.9 ± 0.3	8.8 ± 0.4	1010 ± 50	8.9 ± 0.5
	TU1159-H160084	120	ENACW	35.74	12.84	247	7.6 ± 0.3	8.8 ± 0.3	1030 ± 40	8.6 ± 0.5
	TU1160-H160083	250	ENACW	35.69	12.39	245	8.0 ± 0.3	8.8 ± 0.3	1030 ± 40	9.1 ± 0.5
	TU1149-H160082	800	IcSPMW	35.72	10.51	182	4.9 ± 0.3	8.3 ± 0.3	980 ± 40	5.9 ± 0.4
	TU1137-H160081	1150	IcSPMW	35.86	9.45	188	3.9 ± 0.2	8.7 ± 0.3	970 ± 40	4.4 ± 0.3
	TU1127-H160073	2000	LSW	35.03	3.82	258	2.6 ± 0.2	6.3 ± 0.3	720 ± 40	4.2 ± 0.4
	TU1129-H160072	3000	NEADW$_L$	34.95	2.65	249	0.2 ± 0.2	1.2 ± 0.2	140 ± 20	2 ± 2
	TU1130-H160071	4000	NEADW$_L$	34.91	2.19	243	0.2 ± 0.2	0.3 ± 0.2	40 ± 20	6 ± 7
	TU1131-H160070	4885	NEADW$_L$	34.90	2.05	243	0.5 ± 0.1			
	TU1132-H160069	5334	NEADW$_L$	34.90	2.04	244	1.6 ± 0.1			
Surface 2 44°43.46' N 18°10.34' W	TU1161-H160215	5	ENACW				8.9 ± 0.3	8.5 ± 0.4	990 ± 40	10.4 ± 0.6
Station 21 46°32.65' N 19°40.32' W Bottom depth: 4515 m	TU1162-H160124	5	ENACW	35.69	14.45	277	8.7 ± 0.2	8.6 ± 0.5	990 ± 60	10.2 ± 0.6
	TU1163-H160214	12	ENACW	35.69	14.45	277	9.1 ± 0.3	8.5 ± 0.4	970 ± 50	10.7 ± 0.6
	TU1164-H160213	50	ENACW	35.62	12.72	266	9.9 ± 0.3	8.5 ± 0.4	980 ± 50	11.6 ± 0.6
	TU1165-H160121	100	ENACW	35.66	12.52	254	8.8 ± 0.2	8.1 ± 0.3	940 ± 40	10.9 ± 0.5
	TU1166-H160212	200	ENACW	35.64	12.03	248	9.8 ± 0.3	8.4 ± 0.4	960 ± 40	11.7 ± 0.6
	TU1170-H160104	450	ENACW	35.51	11.06	252	10.3 ± 0.2	9.1 ± 0.5	1060 ± 60	11.2 ± 0.6
	TU1167-H160105	800	IcSPMW	35.31	9.03	188	8.6 ± 0.2	8.6 ± 0.4	980 ± 40	10.0 ± 0.5
	TU1168-H160096	1500	LSW	35.00	4.40	259	8.4 ± 0.2	7.9 ± 0.5	970 ± 60	10.6 ± 0.6
	TU1138-H160068	2300	LSW	34.92	3.22	273	5.5 ± 0.2	7.9 ± 0.3	930 ± 40	7.0 ± 0.4
	TU1150-H160067	2750	ISOW	34.94	2.86	267	4.4 ± 0.2	6.4 ± 0.3	780 ± 40	6.8 ± 0.5
	TU1133-H160066	4000	NEADW$_L$	34.92	2.22	242	0.6 ± 0.2	0.6 ± 0.2	80 ± 20	9 ± 4
	TU1139-H160065	4474	NEADW$_L$	34.91	2.16	240	1.1 ± 0.2	0.6 ± 0.2	80 ± 20	17 ± 6
Surface 3 47°17.39' N 20°15.71' W	TU1171-H160219	5	ENACW				10.9 ± 0.4	7.9 ± 0.4	920 ± 50	13.9 ± 0.8
Station 26 50°16.67' N 22°36.28' W Bottom depth: 4130 m	TU1172-H160125	5	ENACW	35.31	11.52	282	13.3 ± 0.2	8.8 ± 0.4	1000 ± 50	15.1 ± 0.7
	TU1173-H160218	25	ENACW	35.31	11.52	282	12.9 ± 0.3	8.2 ± 0.5	950 ± 60	16 ± 1
	TU1174-H160217	50	ENACW	35.19	9.85	291	16.7 ± 0.3	8.1 ± 0.5	970 ± 60	21 ± 1
	TU1205-H160117	100	ENACW	35.17	9.45	284	19.2 ± 0.3	8.1 ± 0.3	940 ± 40	23.7 ± 0.9
	TU1206-H160216	250	SAIW	35.14	8.67	265	20.4 ± 0.4	9.3 ± 0.4	1060 ± 40	21.9 ± 0.9
	TU1188-H160111	500	IcSPMW	34.99	6.69	211	15.9 ± 0.3	8.3 ± 0.4	970 ± 50	19 ± 1
	TU1183-H160106	1000	LSW	34.96	4.40	263	13.4 ± 0.2	8.2 ± 0.4	1020 ± 50	16.3 ± 0.9
Surface 4 52°7.99' N 24°3.50' W	TU1184-H160222	5	SAIW				14.9 ± 0.3	7.8 ± 0.4	890 ± 50	19 ± 1
Station 32 55°30.336' N 26°42.62' W Bottom depth: 3235 m	TU0971-H160126	5	SAIW	35.07	10.16	292	19.9 ± 0.3	7.4 ± 0.6	870 ± 80	27 ± 2
	TU1200-H160221	30	SAIW	35.06	10.02	292	20.5 ± 0.4	8.1 ± 0.3	950 ± 40	25 ± 1
	TU1207-H160116	60	SAIW	35.14	8.85	288	18.9 ± 0.3	9.2 ± 0.3	1040 ± 40	20.6 ± 0.7
	TU1208-H160220	150	SAIW	35.11	8.11	274	20.1 ± 0.4	8.3 ± 0.3	980 ± 40	24.1 ± 0.9
	TU1175-H160097	380	SAIW	35.04	6.70	222	15.7 ± 0.3	8.0 ± 0.4	970 ± 50	19.5 ± 0.9
	TU1201-H160098	600	IcSPMW	34.96	5.02	246	17.8 ± 0.3	9.0 ± 0.2	1060 ± 30	19.8 ± 0.6
	TU1176-H160099	850	LSW	34.93	4.32	267	15.8 ± 0.3	9.1 ± 0.4	1097 ± 50	17.3 ± 0.8

Station	Sample	Depth	Mass	Sal	Temp		V1	±	e1	V2	±	e2	V3	±	e3	V4	±	e4
	TU1202-H160112	1200	LSW	34.91	3.84	277	18.5	±	0.3	9.7	±	0.3	1130	±	40	19.1	±	0.6
	TU1177-H160113	1700	LSW	34.93	3.55	272	12.3	±	0.2	8.8	±	0.4	1030	±	50	14.1	±	0.7
	TU1178-H160064	2250	LSW	34.93	3.11	274	10.7	±	0.3	8.1	±	0.3	960	±	40	13.2	±	0.6
	TU1179-H160063	2650	ISOW	34.96	2.84	271	10.5	±	0.2	8.0	±	0.4	920	±	50	13.2	±	0.7
	TU1180-H160062	3220	ISOW	34.96	2.53	263	13.2	±	0.3	7.0	±	0.3	820	±	40	18.8	±	0.9
Station 38 58°50.56' N 31°15.97' W Bottom depth: 1345 m	TU1189-H160230	5	IcSPMW	35.06	9.24	296	16.7	±	0.3	8.7	±	0.4	1030	±	50	19	±	1
	TU1190-H160229	20	IcSPMW	35.06	9.23	296	16.7	±	0.3	9.8	±	0.3	1170	±	50	17.0	±	0.7
	TU1193-H160228	60	IcSPMW	35.08	7.95	291	17.4	±	0.3	8.8	±	0.3	1010	±	40	19.7	±	0.8
	TU1203-H160227	110	IcSPMW	35.10	7.45	273	18.7	±	0.4	8.7	±	0.3	1010	±	40	21.4	±	0.9
	TU1204-H160226	300	IcSPMW	35.11	7.19	273	19.1	±	0.4	9.0	±	0.2	1040	±	30	21.3	±	0.7
	TU1209-H160225	650	IcSPMW	35.06	5.94	234	15.5	±	0.3	9.3	±	0.3	1050	±	40	16.6	±	0.7
	TU1210-H160224	1000	LSW	34.99	4.33	262	18.3	±	0.4	9.6	±	0.2	1070	±	30	19.1	±	0.6
	TU1213-H160223	1336	ISOW	34.99	3.90	267	21.4	±	0.5	9.3	±	0.3	1100	±	40	23	±	1
Surface 5 59°16.77' N 35°33.64' W	TU1194-H160277	5	IrSPMW				16.8	±	0.3	8.9	±	0.4	1030	±	40	19.0	±	0.8
Station 44 59°37.36' N 38°57.234' W Bottom depth: 2929 m	TU1217-H160276	5	IrSPMW	34.85	6.86	318	19.4	±	0.3	9.4	±	0.3	1120	±	40	20.6	±	0.8
	TU1260-	5	IrSPMW	34.85	6.86	318				9	±	3	*1040	±	330			
	TU1195-H160275	20	IrSPMW	34.85	6.85	318	17.2	±	0.3	9.9	±	0.4	1170	±	50	17.4	±	0.8
	TU1218-H160274	40	IrSPMW	34.88	4.62	306	20.9	±	0.3	9.2	±	0.3	1090	±	40	22.8	±	0.9
	TU1219-H160273	80	IrSPMW	34.90	4.30	295	19.5	±	0.3	9.1	±	0.3	1070	±	40	21.5	±	0.7
	TU1196-H160272	150	IrSPMW	34.90	4.05	298	18.4	±	0.3	9.2	±	0.3	1090	±	40	20.0	±	0.8
	TU1220-H160271	300	LSW	34.90	3.94	298	22.5	±	0.4	9.9	±	0.3	1130	±	30	22.8	±	0.7
	TU1221-H160253	850	LSW	34.87	3.62	292	24.5	±	0.4	9.6	±	0.7	1160	±	80	25	±	2
	TU1185-H160254	1400	LSW	34.93	3.57	273	10.5	±	0.2	9.2	±	0.4	1070	±	50	11.4	±	0.5
	TU1186-H160255	1800	LSW	34.93	3.26	274	14.3	±	0.2	9.5	±	0.3	1070	±	40	15.1	±	0.5
	TU1191-H160256	2250	ISOW	34.93	2.86	276	15.5	±	0.3	8.6	±	0.3	1000	±	40	18.0	±	0.7
	TU1248-H160308	2600	ISOW	34.92	2.44	282	38.7	±	0.6	10	±	1	*1180	±	130	40	±	4
	TU1261-H160307	2875	DSOW	34.88	1.17	308	98	±	2	9	±	4	*1090	±	420	110	±	40
	TU1262-H160306	2909	DSOW	34.89	1.06	309	99	±	2	11	±	3	*1280	±	310	90	±	20
Station 53 59°53.86' N 43°0.33' W Bottom depth: 193 m	TU1265-H160285	5	PIW	31.90	-0.68	423	256	±	4	16	±	2	*2050	±	310	160	±	20
	-H160284	25	PIW	32.10	-1.18	417	247	±	5									
	TU1267-H160283	50	PIW	32.95	-1.52	364	236	±	8	12	±	4	*1570	±	510	200	±	60
Station 60 59°47.96' N 42°00.78' W Bottom depth: 1719 m	TU1214-H160282	5	IrSPMW	34.83	6.94	325	19.0	±	0.3	8.9	±	0.2	1040	±	30	21.4	±	0.6
	TU1197-H160281	25	IrSPMW	34.98	6.56	314	17.0	±	0.3	8.6	±	0.3	1030	±	40	19.6	±	0.7
	TU1192-H160280	50	IrSPMW	35.01	6.27	303	16.6	±	0.3	8.3	±	0.5	1020	±	60	20	±	1
	TU1198-H160279	100	IrSPMW	35.02	5.97	291	17.1	±	0.3	8.9	±	0.3	1020	±	40	19.3	±	0.7
	TU1224-H160278	200	IrSPMW	34.96	5.20	287	18.4	±	0.3	8.9	±	0.4	1030	±	50	20.8	±	0.9
	TU1215-H160268	500	IrSPMW	34.94	4.45	280	22.8	±	0.5	9.5	±	0.4	1140	±	50	24	±	1
	TU1216-H160257	750	IrSPMW	34.90	3.85	286	21.3	±	0.4	9.3	±	0.3	1120	±	40	22.8	±	0.8
	TU1225-H160258	1000	LSW	34.92	3.77	278	23.1	±	0.5	13	±	2	*1600	±	210	18	±	2
	TU1229-H160259	1190	LSW/ISOW	34.93	3.61	277	25.6	±	0.4	9.5	±	0.9	*1210	±	120	27	±	3
	-H160260	1500	LSW/ISOW	34.92	3.16	281	30.3	±	0.5									
	TU1242-H160305	1672	LSW/ISOW	34.92	3.00	281	36.1	±	0.6	9	±	1	*1100	±	180	40	±	6
	TU1243-H160304	1712	LSW/ISOW	34.91	2.94	284	37.4	±	0.6	8.7	±	0.9	*1080	±	120	43	±	5
Station 61 59°45.21' N 45°6.74' W Bottom depth: 144 m	TU1263-H160296	5	SAIW	32.40	0.07	412	219	±	4	15	±	3	1940	±	340	140	±	30
	TU1268-H160290	25	SAIW	32.63	-0.41	402	244	±	4									
	TU1269-H160289	50	SAIW	32.81	-0.65	383	251	±	4									
Station 64 59°4.30' N 46°5.29' W Bottom depth: 2473 m	TU1236-H160288	5	IrSPMW	34.81	6.71	317	24.7	±	0.4	9	±	1	*1060	±	160	29	±	4
	TU1226-H160287	25	IrSPMW	34.81	6.68	317	21.5	±	0.4	12	±	1	*1370	±	140	19	±	2
	TU1227-H160286	50	IrSPMW	34.86	6.13	319	18.4	±	0.3	11	±	1	*1480	±	180	16	±	2
	TU1230-H160261	100	IrSPMW	34.95	5.37	294	22.2	±	0.4	11	±	1	*1390	±	140	20	±	2
	-H160262	200	IrSPMW	34.94	4.79	289	29.2	±	0.5									
	TU1231-H160267	450	LSW	34.92	4.22	288	26.8	±	0.5	9	±	1	*1080	±	140	30	±	4
	TU1232-H160100	900	LSW	34.87	3.60	295	24.7	±	0.4	7.9	±	0.8	*970	±	100	31	±	3
	TU1244-H160088	1150	LSW	34.91	3.71	281	23.7	±	0.4									
	TU1222-H160089	1400	LSW	34.93	3.55	274	21.0	±	0.3	9.8	±	0.3	1130	±	40	21.3	±	0.7
	TU1238-H160090	1800	LSW	34.92	3.05	278	27.7	±	0.4	9	±	1	*1070	±	120	31	±	4
	TU1228-H160303	2150	ISOW	34.93	2.70	278	20.9	±	0.3	11	±	1	*1300	±	150	19	±	2
	TU1249-H160302	2462	DSOW	34.90	2.15	291	56.2	±	0.9	9.5	±	0.9	*1160	±	110	60	±	6
Surface 6 56°44.79' N 47°31.31' W	TU1239-H160231	5	LSW				30.9	±	0.5									
Station 69 55°50.50' N 48°5.59' W Bottom depth: 3678 m	TU1250-H160232	5	LSW	34.62	6.24	326	48.8	±	0.8									
	TU1254-H160233	25	LSW	34.67	3.72	324	49.9	±	0.8	9	±	3	1060	±	350	60	±	20
	TU1264-H160234	50	LSW	34.79	3.78	297	41.8	±	0.7	5	±	3	*640	±	320	80	±	40
	-H160239	100	LSW	34.83	3.81	296	32.9	±	0.6									
	TU1240-H160	200	LSW	34.84	3.62	298	29.8	±	0.5	9	±	2	*1080	±	190	32	±	6
	TU1272101-H160	500	LSW	34.86	3.49	296	29.3	±	0.5	7	±	2	*820	±	290	40	±	20
	TU1273-H109160	1000	LSW	34.85	3.39	296	26.0	±	0.4									
	TU1274-H160092	1800	LSW	34.92	3.57	274	17.6	±	0.3	5	±	2	*620	±	300	30	±	20
	TU1275-H160241	2200	LSW	34.92	3.22	275	20.0	±	0.4	8	±	3	*940	±	330	26	±	9
	TU1233-H160093	2800	ISOW	34.92	2.70	279	24.5	±	0.4	8.9	±	0.9	1070	±	110	28	±	3
	TU1251-H160301	3500	ISOW	34.91	1.75	294	72	±	1	15	±	2	*1770	±	270	49	±	8
	TU1255-H160300	3659	DSOW	34.90	1.47	299	85	±	1	19	±	3	*2230	±	340	44	±	7

Station	Sample	Depth (m)	Water mass	Salinity	Temp		Value	±	err	Value	±	err	Value	±	err	Value	±	err
Surface 7 53°40.18' N 49°29.49' W	TU1277-H160269	5	LSW				31.6	±	0.5	10.2	±	0.5	1220	±	70	31	±	2
Surface 8 52°46.17' N 51°48.26' W	TU1278-H160270	5	SAIW/PIW				71	±	1	15.7	±	0.9	2090	±	140	45	±	3
Station 77 52°59.98' N 51°6.01' W Bottom depth: 2522 m	TU1245-H160242	5	LSW	34.47	7.28	324	37.9	±	0.6	9	±	1	*1040	±	170	45	±	7
	-H160243	25	LSW	34.63	5.30	334	32.2	±	0.6									
	TU1279-H160244	50	LSW	34.74	3.57	312	32.3	±	0.6	10.4	±	0.4	1230	±	50	31	±	1
	TU1246-H160245	100	LSW	34.79	3.42	304	32.4	±	0.6	9	±	1	*1040	±	170	38	±	6
	TU1280-H160246	200	LSW	34.83	3.46	299	30.9	±	0.5	10.4	±	0.4	1210	±	50	30	±	1
	TU1281-H160102	650	LSW	34.86	3.46	294	27.0	±	0.4	10.3	±	0.4	1190	±	50	26	±	1
	TU1284-H160247	950	LSW	34.87	3.41	294	24.1	±	0.4	10.6	±	0.3	1240	±	50	22.7	±	0.8
	TU1234-H160094	1250	LSW	34.91	3.54	279	22.8	±	0.4	9.5	±	0.9	*1130	±	100	24	±	2
	TU1282-H160299	1700	LSW	34.92	3.12	276	21.7	±	0.4	9.8	±	0.5	1140	±	70	22	±	1
	TU1285-H160095	2200	ISOW	34.92	2.60	280	35.5	±	0.6	10.6	±	0.3	1270	±	50	34	±	1
	TU1252-H160298	2477	ISOW	34.91	2.18	285	48.7	±	0.8	8	±	3	*1030	±	310	60	±	20
	TU1286-H160297	2500	ISOW	34.91	2.09	287	47.0	±	0.8	12.1	±	0.6	1400	±	70	39	±	2
Station 78 51°59.33' N 53°40.01' W Bottom depth: 377 m	TU1256-H160248	5	PIW	31.79	5.17	342	75	±	1	16	±	4	*2110	±	500	50	±	10
	TU1257-H160249	25	PIW	32.86	-0.57	452	77	±	1	19	±	3	*2350	±	370	41	±	6
	TU1270-H160250	50	PIW	33.06	-1.46	340	74	±	1	12	±	4				60	±	20
	TU1258-H160251	200	PIW	34.08	0.77	308	64	±	1	11	±	2	*1380	±	280	60	±	10
	TU1287-H160252	367	PIW	34.62	2.92	283	44.2	±	0.8	11.2	±	0.5	1350	±	70	40	±	2
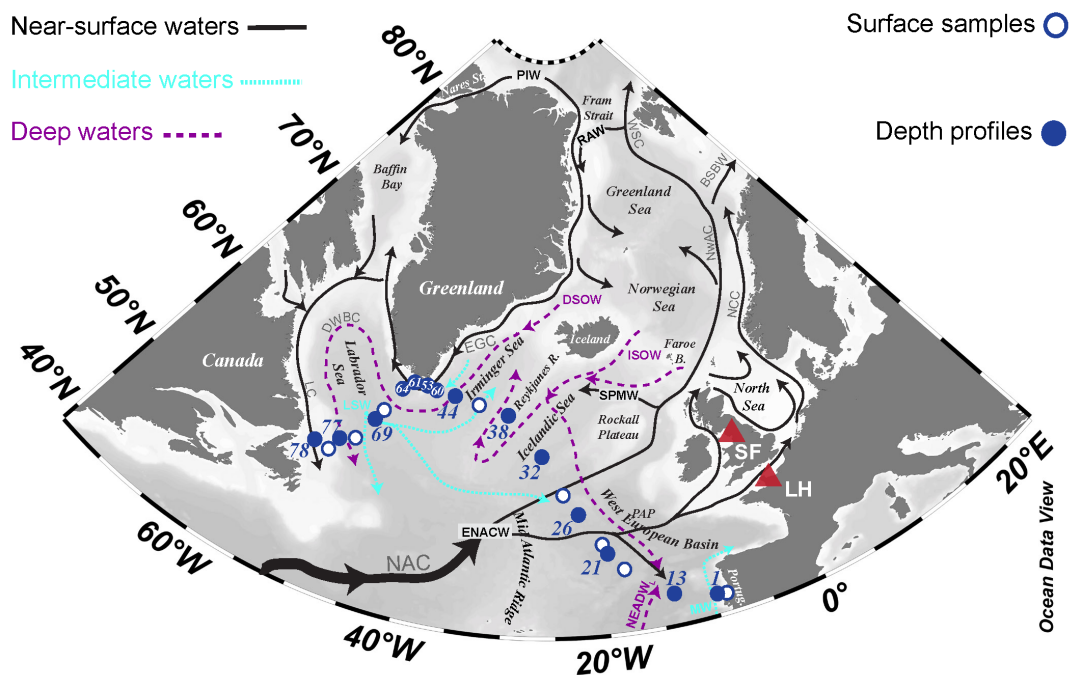
Figure 1. Sampled locations in the subpolar North Atlantic during the GEOVIDE cruise in spring 2014. Nuclear fuel reprocessing plants of La Hague (LH) and Sellafield (SF) are represented along with main water masses and their schematic spreading pathways adapted from Daniault et al., (2016) and Smith et al., (2005). Acronyms are defined in Table 1.
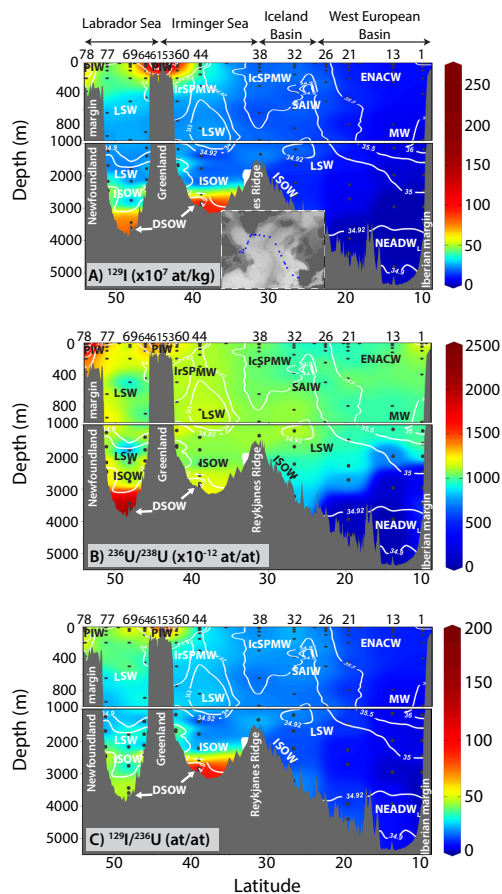
Figure 2. Vertical distribution of (A) ^{129}I concentrations, and atom ratios of (B) ^{236}U/^{238}U and (C) ^{129}I/^{236}U. Isohalines are overlaid to represent the water mass structure reported by García-Ibáñez et al., (2018). Acronyms are defined in Table 1.
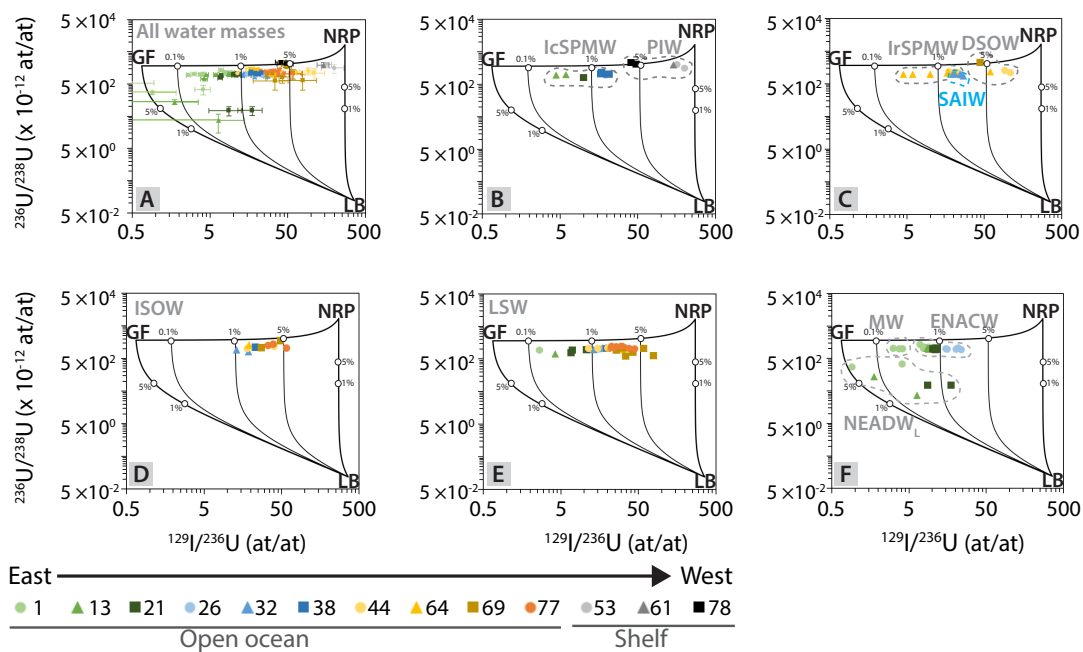
Figure 3. Binary mixing lines between global fallout (GF), European nuclear fuels reprocessing plants (NRP) and the lithogenic background (LB) allow estimating the contribution from these three sources to the presence of ^{129}I and ^{236}U in the subpolar North Atlantic. Further description on the binary mixing model is provided elsewhere (Casacuberta et al., 2016; Christl et al., 2015b). The ^{129}I/^{236}U and ^{236}U/^{238}U atom ratios are plotted for (A) each station, and for the main water masses (B to F). Diagram A also shows the data uncertainties. Acronyms are defined in Table 1.
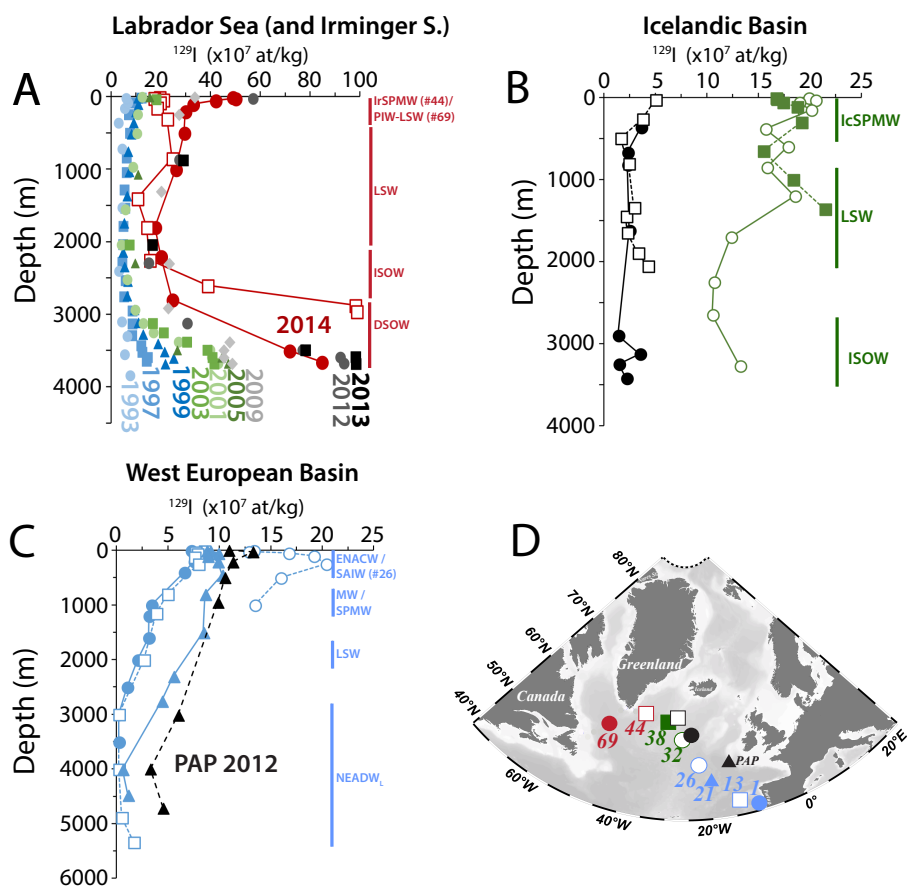
Figure 4. Vertical profiles of (A) ^{129}I concentrations in the Labrador and Irminger Seas (this work (red) and Edmonds et al., 2001; Orre et al., 2010; Smith et al., 2005, 2016), (B) the Icelandic Basin (this work (green) and Edmonds et al., 2001 (black)), (C) the West European Basin (this work (blue) and Vivo-Vilches et al., 2018 (black)), and (D) map with locations for each station. Acronyms are defined in Table 1.
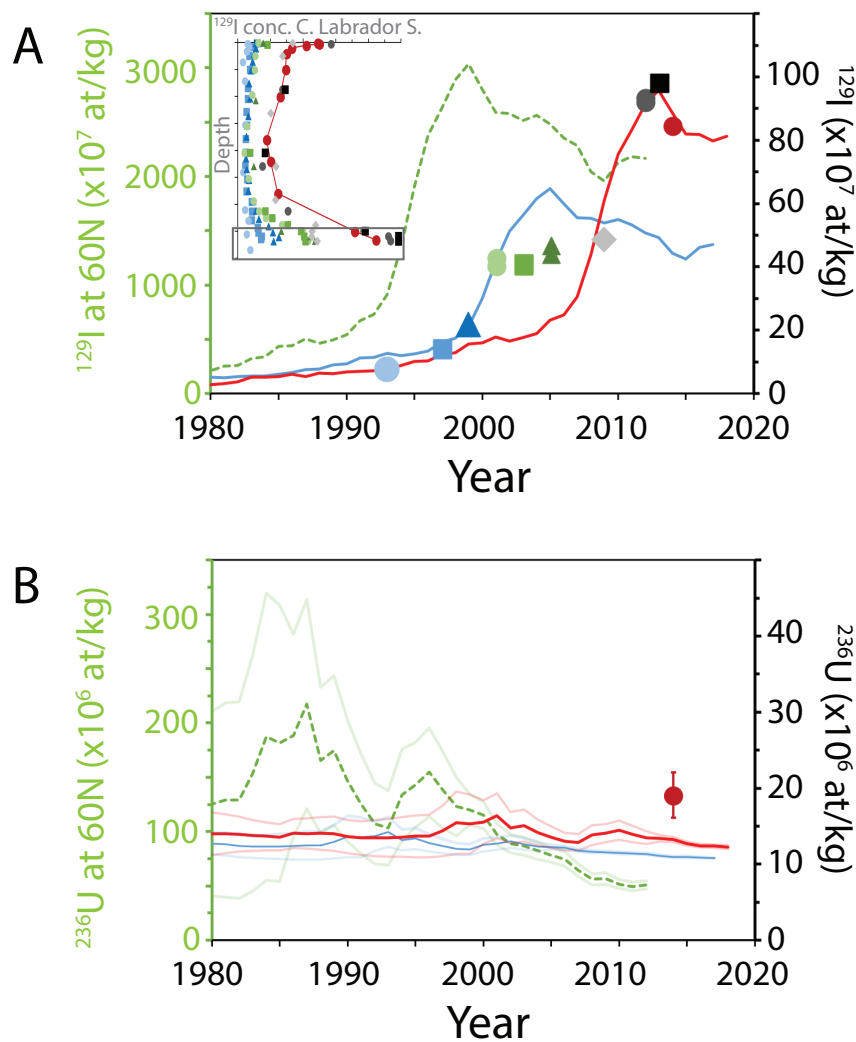
Figure 5. A) Concentrations of ^{129}I in the bottom of the central Labrador Sea. Measurements are from this work (red dots, 2014); Edmonds et al. (2001) for 1993; Smith et al. (2005, 2016) for 1997, 1999, 2001, 2012 and 2013; and Orre et al. (2010) for 2003, 2005 and 2009. The ^{129}I input function from reprocessing plants was calculated for 60 ºN in Christl et al. (2015b). The blue and red lines

5 **correspond to the same input function that has been diluted and delayed in time to fit the measurements. B) Same as (A) but for ^{236}U. The uncertainties of the ^{236}U input functions are also shown with corresponding, more clear colours. The ^{236}U measurement is from this study.**